JGR Oceans

RESEARCH ARTICLE
10.1029/2019JC015851

Key Points:
- Strong mixing brought deep cool water upward to produce a cold wake and led a rapid change of latent heat flux into hurricane
- Enhanced air-sea flux exchange in hurricane caused a drop of sea surface air temperature and hence central air pressure
- Including an oceanic mixed layer in WRF can significantly improve the simulation of hurricane intensity and pathway

Correspondence to:
S. Li,
sli4@umassd.edu

Citation:
Li, S., Chen, C., Wu, Z., Beardsley, R. C., & Li, M. (2020). Impacts of oceanic mixed layer on hurricanes: A simulation experiment with Hurricane Sandy. *Journal of Geophysical Research: Oceans*, *125*, e2019JC015851. https://doi.org/10.1029/2019JC015851

Received 6 NOV 2019
Accepted 6 OCT 2020
Accepted article online 7 OCT 2020

Impacts of Oceanic Mixed Layer on Hurricanes: A Simulation Experiment With Hurricane Sandy

Siqi Li[1], Changsheng Chen[1], Zhongxiang Wu[1], Robert C. Beardsley[2], and Ming Li[3]

[1]School for Marine Science and Technology, University of Massachusetts Dartmouth, New Bedford, MA, USA, [2]Department of Physical Oceanography, Woods Hole Oceanographic Institution, Woods Hole, MA, USA, [3]Horn Point Lab, University of Maryland Center for Environmental Science, Cambridge, MD, USA

Abstract Influences of the ocean mixed layer (OML) dynamics on intensity, pathway, and landfall of October 2012 Hurricane Sandy were examined through an experiment using the Weather Research and Forecasting (WRF) model. The WRF model was run for two cases with or without coupling to the OML. The OML in the WRF was calculated by an oceanic mixed layer submodel. The initial conditions of the depth and mean water temperature of the OML were specified using Global-FVCOM and Global-HYCOM fields. The comparison results between these two cases clearly show that including the OML dynamics enhanced the contribution of vertical mixing to the air-sea heat flux. When the hurricane moved toward the coast, the local OML rapidly deepened with an increase of storm wind. Intense vertical mixing brought cold water in the deep ocean toward the surface to produce a cold wake underneath the storm, with the lowest sea temperature at the maximum wind zone. This process led to a significant latent heat loss from the ocean within the storm and hence rapid drops of the air temperature and vapor mixing ratio above the sea surface. As a result, the storm was intensified as the central sea level pressure dropped. Improving air pressure simulation with OML tended to reduce the storm size and strengthened the storm intensity and hence provided a better simulation of hurricane pathway and landfall.

Plain Language Summary Tropical and extratropical storms are two major types of extreme weather events generating flood risk along the U.S. eastern coast. Hurricane Sandy was a storm attacking the Middle Atlantic Bight coast in 2012, with a total loss of $70 billion in the economy. Taking Hurricane Sandy, for example, we examined the influences of the oceanic mixed layer (OML) on the storm's intensity and pathway over the continental shelf. We found that when the hurricane moved toward the coast, the local OML rapidly deepened with storm wind. Intense vertical mixing brought cold water in the deep ocean toward the surface to produce a cold wake underneath the storm. This process led to a significant latent heat loss from the ocean to the air within the storm and hence rapid drops of the air temperature and vapor mixing ratio at the sea surface. As a result, the hurricane intensified as the central sea level pressure dropped. Improving air pressure simulation with OML tended to reduce the storm size and strengthened the wind intensity and hence provided a better simulation of hurricane pathway and landfall. Our finding highlighted a critical need to improve storm forecast weather model by including air-sea interaction processes.

1. Introduction

The Weather Research and Forecasting (WRF) is one of the most popular mesoscale meteorological models, which has been widely used in regional weather forecast operations (Skamarock et al., 2008). The Advanced Research WRF model (WRF-ARW, for simplification, referred to as WRF here), maintained by the Mesoscale and Microscale Meteorology Laboratory (MMM) of National Center for Atmospheric Research (NCAR), has been upgraded with improvements in its capability of simulating and predicting tropical storms or hurricanes (Davis et al., 2008; Gopalakrishnan et al., 2006; Zou & Xiao, 2000). The WRF model has demonstrated its success in predicting the intensity and pathway of extratropical storms (Beardsley et al., 2013; C. Chen, Beardsley, et al., 2013), but results for hurricane simulations differ substantially in terms of capturing the maximum wind velocity and minimum central sea level pressure (MSLP) as well as its track and landfall location (Glenn et al., 2016).

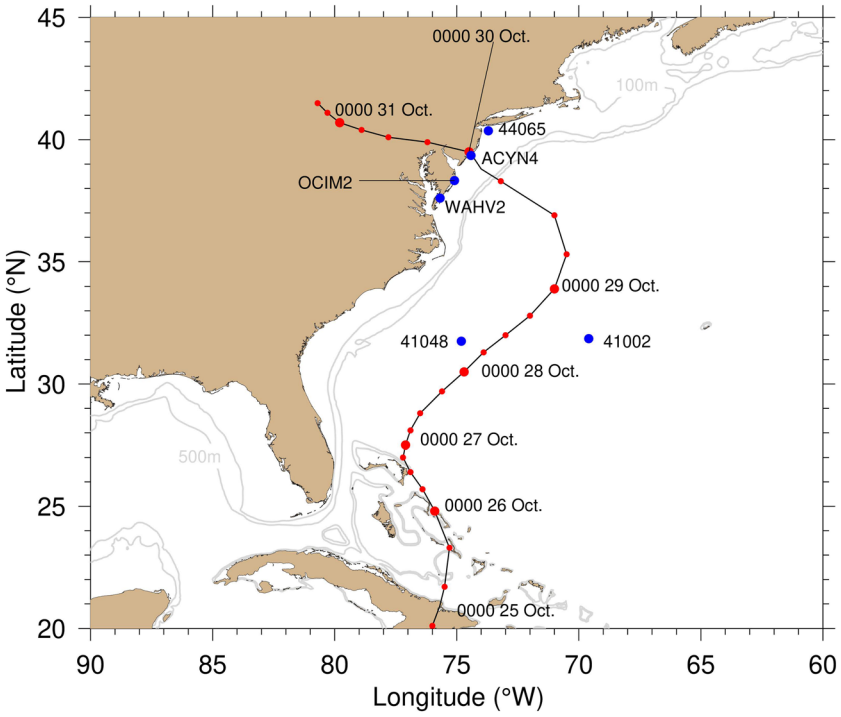

Figure 1. The pathway of Hurricane Sandy (black line) recorded over a 6-h interval during the period from 0000 UTC 25 October 2012 to 1200 UTC 31 October 2012. Blue dot: Location of the meteorological buoy. The symbol close to the blue dot is the name of the buoy. Red dot: the location of the hurricane over a 6-h interval. All the time and dates are in UTC.

Various studies have reported that the performance of WRF for storm and hurricane forecasts depends on air-sea interactions, atmosphere boundary layer parameterizations, and grid resolution (Fierro et al., 2009; Jacob et al., 2000). When a hurricane moves over the ocean, it typically produces a cold wake in the upper ocean mixed layer (OML). This cold wake generally lasts for ~5 days, influencing both hurricane intensity and tracks (Dare & McBride, 2011). There are three approaches to take the OML effects into account: (1) including either satellite-derived or ocean model-produced sea surface temperatures (SSTs) (Cione & Uhlhorn, 2003; Zeng & Beljaars, 2005), (2) implementing an OML model (Davis et al., 2008; Lin et al., 2013; Pollard et al., 1972; Price, 2009; Wang & Duan, 2012), and (3) coupling with an ocean model (S. S. Chen, Zhao, et al., 2013; Lee & Chen, 2014; Lin et al., 2005, 2008, 2009; Warner et al., 2010; Wu et al., 2007, 2016). Also, some studies applied climatological forecast SSTs to investigate how global warming could affect the intensity of hurricanes (Zhang & Li, 2019). These studies have shown that it is essential to include the OML into WRF, especially for hurricane simulation (Mooney et al., 2016).

Hurricane Sandy, struck the eastern coast of the United States in October 2012, was one of the tropical storms in history, and caused severe disasters in the coastal region (Figure 1). It first appeared as a low-pressure cyclone, quickly strengthened into Tropical Storm Sandy over the Caribbean Sea on 22 October, and then upgraded to a hurricane after moving northward and crossing Jamaica and Cuba on 26 October. Hurricane Sandy made landfall near Brigantine, New Jersey, at 2330 UTC 29 October, at which it turned to a posttropical cyclone (Blake et al., 2013). This hurricane produced strong winds (with a maximum gust of ~43 m s^{-1}), high water, and surge levels of ~4.4 and ~3.0 m, and significant wave height of ~10 m, causing severe coastal inundation over New Jersey, New York City, and Long Island Sound (Diakakis et al., 2015).

Several modeling studies were conducted to simulate Hurricane Sandy in the past (Miles et al., 2017; Shin & Zhang, 2017; Zambon et al., 2014). Zambon et al. (2014) found that the Hurricane Sandy track depended more on the averaged atmospheric circulation during its transition from a tropical cyclone to an extratropical storm. By combining observational data and a regional ocean model, Miles et al. (2017) believed that the

storm-induced cross-shelf advection directly influenced the storm-generated cold pool over the continental shelf. Shin and Zhang (2017) simulated the four stages of Hurricane Sandy and found that the low-stratospheric warm air caused the sea level pressure to decrease before the landfall. We made efforts to use WRF for the Hurricane Sandy simulation. No matter which planetary boundary layer (PBL) and grid design/resolution, as well as the satellite-derived SST, were used, the WRF-simulated hurricane showed a significant bias in its central sea level pressure, pathway, and timing of landfall. Taking this hurricane as an example, we examined alternative physical processes controlling the intensity, path, and landfall of Hurricane Sandy, particularly the role of the OML dynamics. Besides, we evaluated the WRF performance for hurricane simulation with cumulus parameterization, PBL schemes, and grid design/resolution (Appendix A).

The remaining sections are organized as follows. Section 2 describes the model and design of numerical experiments, including the default model configuration, forcing, sea surface boundary conditions, and the model validation data. Section 3 presents the simulation results by comparing the cases with or without the inclusion of the oceanic mixed layer, focusing on understanding how OML dynamics attributed to storm intensification. In section 4, conclusions of significant findings are summarized, following with discussions on some existing issues of the WRF model. In Appendix A, the discussions are given on the sensitivity of the WRF-simulated hurricane to different PBL parameterizations and various configurations of computational domain and grid resolution.

2. The Model, Experiment Designs, and Data

In this study, the WRF model was first configured by three two-way nesting domains with grid resolutions of 27, 9, and 3 km in the horizontal, respectively, and a total of 36 layers bounded at 50 hPa at the top in the vertical (Figure 2a). The details of the model configuration are given in Table 1. To examine how the OML influence the storm's path and intensity before its landfall, a WRF simulation was carried out to cover the period from 0000 UTC 28 October (turned to the northwest) to 0000 UTC 31 October (a few hours after landfall). To examine the impact of the OML on the intensity and pathway of Hurricane Sandy, we did two WRF experiments for the cases with or without the OML.

The OML model used in our WRF simulation was based on the one-dimensional (1-D) model developed by Pollard et al. (1972). It was a temperature-dependent model driven by the local surface wind stress and net heat flux plus the vertical penetration of shortwave irradiance. In this model, however, the horizontal advection in the momentum and temperature equations were neglected. The OML model contained two layers: (1) the upper mixed layer and (2) the lower stratified layer. The deepening of the OML was generated through turbulent shear and buoyancy productions by surface wind stress and cooling, as well as the water entrained through the bottom of the OML. The hurricane wind generalized cyclonic currents, which produced a strong vertical shear of horizontal currents in the upper stratified layer, and hence mixing as Richardson number was less than 1.0. In WRF, since the storm-produced wind stress and heat flux at the sea surface varied with time and in space, the 1-D OML model provided the field of two time-varying and spatially varying variables: h_m (the OML depth) and $\overline{T}_{oml}$ (mean sea temperature of OML, i.e., SST). Hurricane-induced OML deepening increased the air-sea temperature difference and moisture at sea surface and feedback to hurricane through the change of latent and sensible heat flux.

It should be noted that the 1-D OML model did not account for wind curl-produced Ekman pumping. Theoretically, the cyclonic wind curl produces positive vorticity, which could also pump the cold water in the lower stratified layer through the thermocline and bring it into the OML. The hurricane-induced upwelling can be estimated by Ekman pumping over an inertial time scale ($T_f = 2\pi/f$). Over the New England shelf, T_f is ~18.6 h, which was much longer than the time scale of storm-induced mixing. For the Hurricane Sandy case, we estimated Ekman pumping using the storm-induced wind curl. The surface cooling produced by Ekman pumping was much weaker than storm mixing-induced cooling.

The WRF setup with OML requires two initial input fields: (1) h_m and (2) $\overline{T}_{oml}$. In our experiments, the initial fields of h_m and $\overline{T}_{oml}$ were specified using the Global-FVCOM hindcast data set (MEDML, 2013) in Figures 3a and 3c. The Global-FVCOM is a coupled ocean-ice-wave model configured with a horizontal grid resolution of 25 km in the interior, 2 km in the Arctic Ocean, and 5–10 km in the northeast coastal region

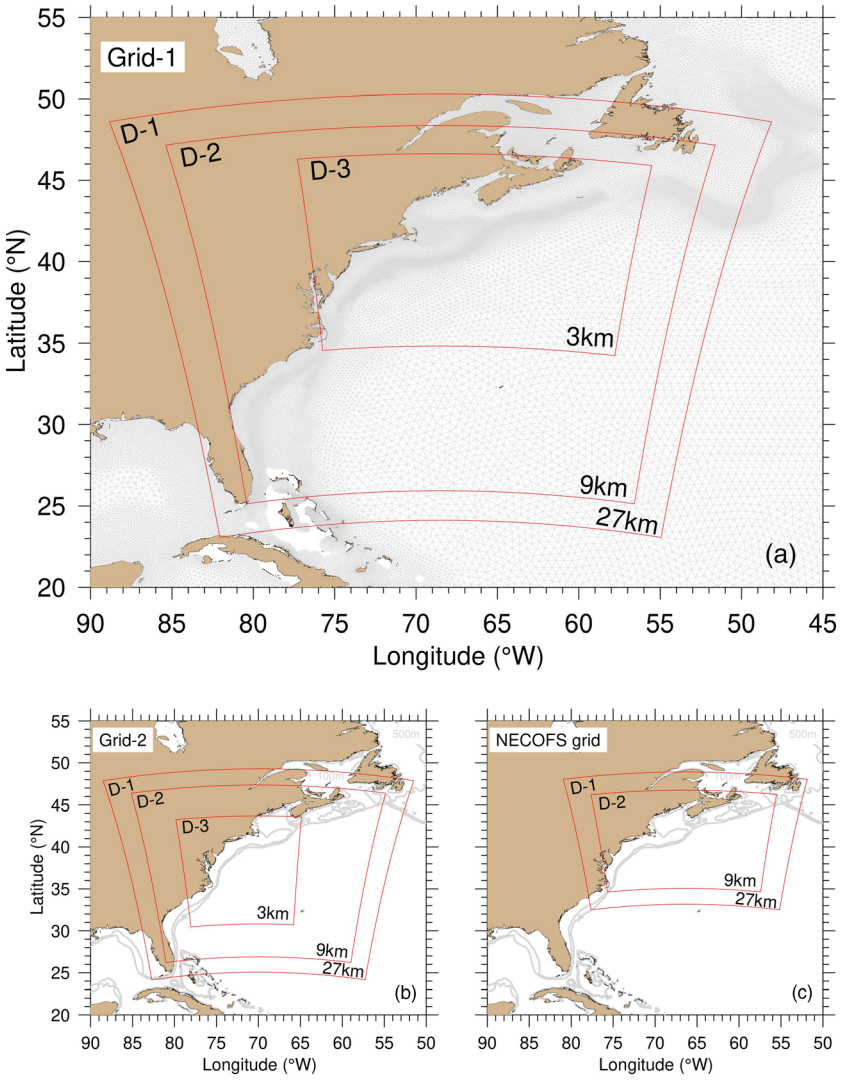

Figure 2. Illustration of the Grid-1 (a), Grid-2 (b), and NECOFS grid (c) WRF model domains. In (a), the triangular mesh is the unstructured grid used in the Global-FVCOM. Symbols named D-1, D-2, and D-3 represent the three two-way nesting domains with the horizontal grid resolutions of 27, 9, and 3 km, respectively. The horizontal grid resolution of the Global-FVCOM in the D-3 domain varied from 2–5 km near the coast to 25 km in the interior.

Table 1
Configuration of the WRF Model for Hurricane Sandy Simulation

Parameters	Domain 1	Domain 2	Domain 3
Grid size (km)	27	9	3
Vertical levels	36	36	36
Microphysics		WSM6	
LW radiation		RRTMG	
SW radiation		RRTMG	
Surface layer		M-O (Janjic)	
Land surface		Thermal diffusion	
PBL		MYJ	
Cumulus	Tiedtke	Tiedtke	No
OML		FVCOM and HYCOM	

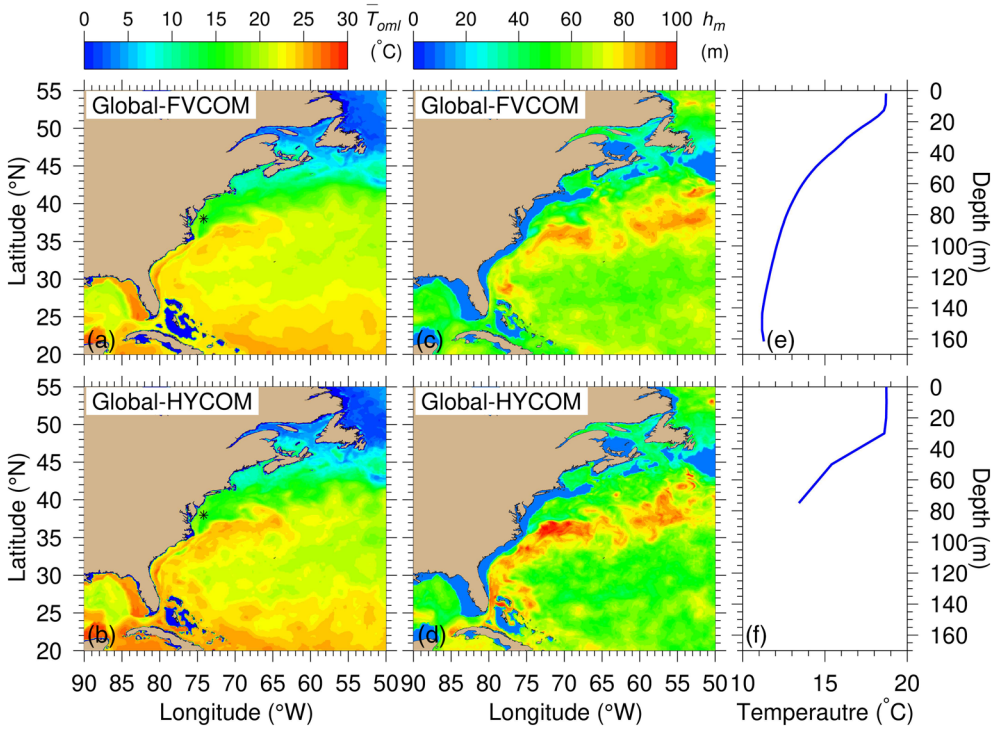

Figure 3. The OML averaged temperature $\overline{T}_{oml}$ (left column), the ocean mixed depth h_m (middle column), and the temperature profile (right column) obtained from the Global-FVCOM (a, c, and e) and Global-HYCOM (b, d, and f). The temperature profiles were selected at the black start points in (a) and (b).

(C. Chen et al., 2016). A hybrid terrain-following coordinate with 45 layers was used in the vertical direction, which prevented numerical errors in the simulation of surface mixed layer and bottom boundary layer dynamics in the interior without losing vertical layer resolution in the shallower coastal regions. The Global-FVCOM was driven by astronomical tidal forcing with eight constituents (M_2, S_2, N_2, K_2, K_1, P_1, O_1, and Q_1), surface wind stress, net heat flux at the surface plus shortwave irradiance in the water column, surface air pressure gradients, precipitation minus evaporation, and river discharge at 766 river mouth locations. Supported by the International Center for Marine Studies (ICMS) at Shanghai Ocean University (SHOU), the Global-FVCOM was validated for 50-year spin-up validation experiments and a 40-year hindcast with assimilation from 1978 to 2017 (C. Chen et al., 2009, 2016; Gao et al., 2011; Zhang, Chen, Beardsley, Gao, Lai, et al., 2016; Zhang, Chen, Beardsley, Gao, Qi, et al., 2016). We also repeated the simulation experiment by using the fields of h_m and $\overline{T}_{oml}$ calculated from the Hybrid Coordinate Ocean Model (HYCOM) hindcast data set (HYCOM.org, 2013) (see Figures 2b and 2d). HYCOM used in this study was the operational global version with the finest grid resolution of ~(1/25)° (Hurlburt et al., 2009). The global-HYCOM is an isopycnal coordinate model with the advantage of keeping the water mass conservative over a long time (Dukhovskoy et al., 2006; Griffies et al., 2009).

Based on both observations and model results, the OML in the tropical and extratropical regions, especially over the New England shelf, is generally less than 150 m. To ensure we captured the OML depth, we first used the top 200-m sea temperature to calculate the mixed layer depth from the Global-FVCOM and HYCOM simulated sea temperature field. The method used to determine the OML was based on the algorithm included in the WRF toolbox. Then, the mean temperature of the OML was calculated, which is the vertically averaged temperature in that layer. Theoretically, the sea temperature does not change with depth in the OML. In reality, however, it does not always remain a vertically uniform profile of sea temperature in the OML. Considering the different vertical resolutions used in the Global-FVCOM and HYCOM, we chose the 200 m as the deepest depth to calculate the OML depth. The Global-FVCOM was configured with the terrain-following hybrid coordinate with 45 layers in the vertical, while HYCOM was an isopycnal coordinate model with temperature output only on standard depths of 0, 10, 20, 30, 50, 75, 100, 125, 150, and

200 m. In the shallow region less than 170 m, the OML in the Global-FVCOM was determined using the temperature profile with a vertical resolution of 15.2 m or less (Figure 3e), while the HYCOM temperature profiles only contained six standard layers or less, with a resolution of ~20 m (Figure 3f). Therefore, due to vertical resolution, the OML depths calculated by the Global-FVCOM and HYCOM significantly differed over the continental shelf.

In all the experiments, the WRF was driven with the initial and boundary conditions taken from the NCEP global FNL data (NOAA/NCEP, 2000) with a 1.0° grid resolution. The observational data for the center track and minimum central pressure of Hurricane Sandy were downloaded from the NCDC International Best Track Archive for Climate Stewardship Project (Knapp et al., 2010). The simulation results were validated by comparing with the observed sea surface air pressure and 10-m wind speed/direction at real-time monitoring stations closed to the Hurricane Sandy track. A total of six monitoring stations from the National Data Buoy Center (NDBC, 1996) was selected, four (Buoy 44065, ACYN4, OCIM2, and WAHV2) near the coastline and two (Buoy 41048 and Buoy 41002) over the continental shelf (Figure 1). Note here that Buoy ACYN4 had no wind records during the period when Hurricane Sandy passed.

3. The Role of OML in Hurricane Simulation

3.1. Comparisons of WRF With Observations for the Cases With and Without OML

Our results showed that including the OML dynamics into the WRF significantly improved the simulation accuracy of the minimum central pressure and, thus, the center track of Hurricane Sandy (Figure 4). The observation showed that Hurricane Sandy arrived at 71°00′W and 33°54′N, with its minimum central pressure of 950 hPa at 0000 UTC 29 October 2012. It turned left to move toward the coast with its minimum central pressure dropping to 940 hPa at 1800 UTC 29 October and then made landfall near Brigantine, New Jersey, at 2130 UTC 29 October (Figure 4a). The minimum central pressure rapidly increased to 960 hPa at 0600 UTC 30 October, about 8 h after landfall. For the case without the OML, the model-simulated path of Hurricane Sandy's center significantly deviated northeastward after 0000 UTC 29 October (Figure 4a). The maximum deviation distance was 176.6 km, with a standard deviation error of 59.3 km (Table 2). As a result, the simulated Hurricane Sandy made landfall about 3 h late (Figure 4a). Correspondingly, the minimum central pressure was considerably overestimated before landfall and underestimated after landfall (Figure 4b). The maximum difference of the minimum central pressure was up to 8.2 hPa, with a standard deviation error of 4.1 hPa.

For the case with the OML, the maximum deviation distance apart from the observed path was reduced to 66.4 km, with a standard deviation error of 17.6 km (Table 2). Compared with the case without the OML, implementing the OML into WRF helped reduce the observed and simulated difference of the hurricane path by 62.4% for the maximum deviation distance and 70.3% for the standard deviation error. The improvement of the model performance for Hurricane Sandy's track is also reflected in the center air pressure simulation. When the OML was not applied, the intensity of the center air pressure was underestimated. It turned out that ignoring the oceanic feedback to the storm at the sea surface made the hurricane center move toward the coast on a long journey with a more significant deviation to the observed track. As a result, the hurricane made landfall with a 3-h time delay compared with the observation. Adding the OML made Hurricane Sandy's central sea level pressure match better with the observations (Figure 4b), with the maximum and standard deviation errors being reduced to 2.9 and 1.1 hPa, respectively. It suggested that improving the simulation accuracy of central sea level pressure made the WRF better to capture the right track of Hurricane Sandy and thus the timing of its landfall. For the coastal community, the storm landfall time prediction is critically essential for the coastal inundation forecast. Over the New England coast, storm-induced coastal inundation is generally produced by storm surge and wave run-up (Beardsley et al., 2013; C. Chen et al., 2013). Storm winds directly drive both surge and wave run-up, and maximum inundation occurred at high tide during the maximum wind period. Since the semidiurnal tide predominates the region, a 3-h delay of hurricane landfall could lead to the inaccuracy in the timing of storm-induced inundation.

A further model-data comparison with observations was made for the 10-m wind speed and direction as well as the sea surface air pressure on six meteorological buoys: Buoy 40148, Buoy 41002, Buoy 44065, ACYN4, OCIM2, and WAHV2 for the cases without and with the OML (Figure 5 and Table 3). Buoy 40148 and Buoy 41002 were in the open ocean region off the shelf break, where hurricane passed by in early

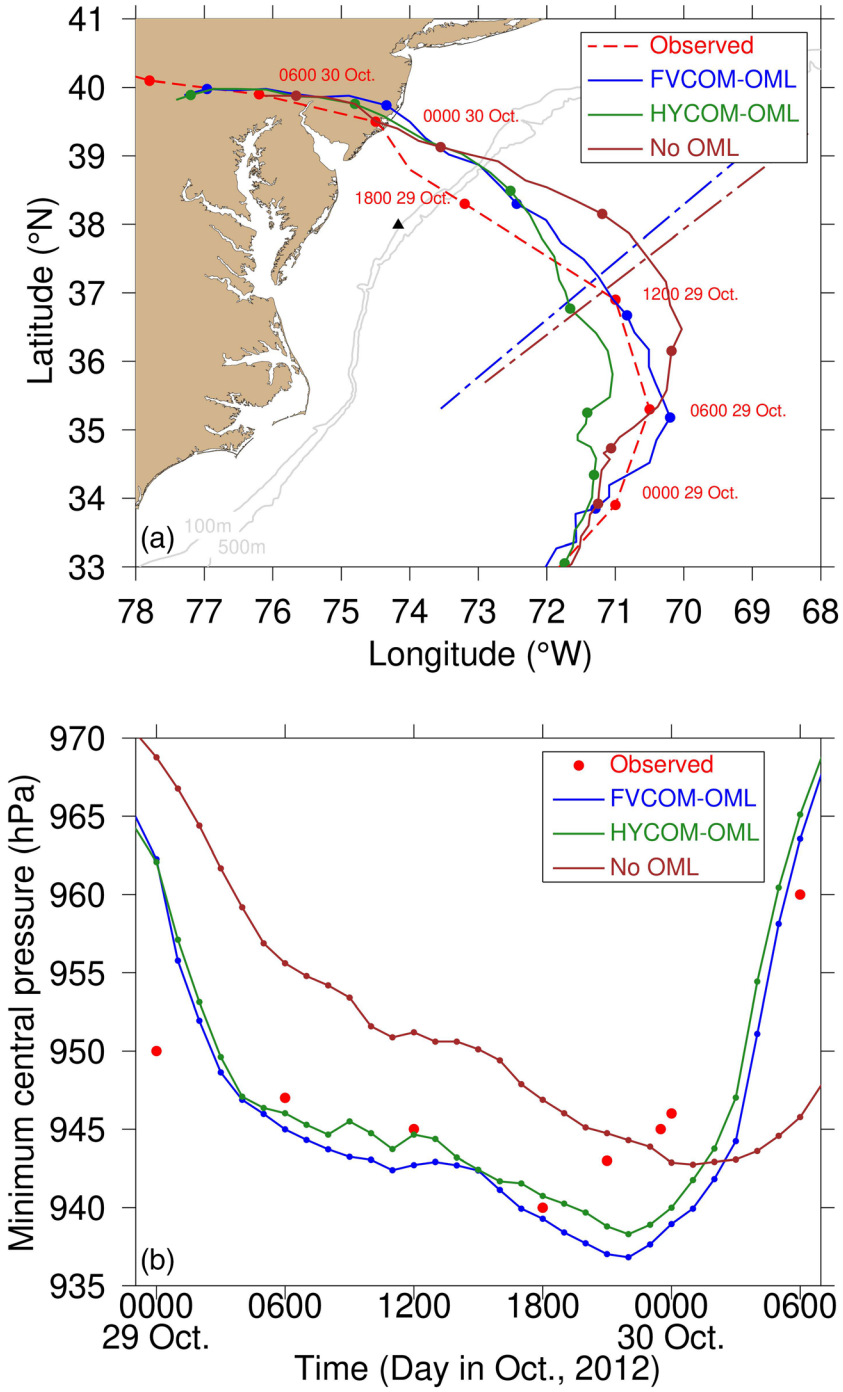

Figure 4. Comparisons between the simulated and observed pathways of Hurricane Sandy (a) and its minimum central pressures (b) for the cases without and with the ocean mixed layer. Labels shown in (a) are the time of the month, day, hour, and minute. In (a), the dash-dotted lines are the selected sections used for Figure 10, and the black filled triangle is the location where the time series (Figure 9) were plotted. All the time and dates are in UTC.

mooring of 28 October. The results with the OML did not show any improvement in the simulated wind speed/direction and air pressure at these two deep-water buoys. Buoy 44065, ACYN4, OCIM2, and WAHV2 were located near the coast. Facing the onshore movement of Hurricane Sandy, Buoy 44065 and ACYN4 were on the right side and OCIM2 and WAHV2 on the left side. Adding the OML reduced the simulation standard deviation errors of the wind speed (in the range of 17.5–30.1%), wind direction (in the range of 36.2–51.4%), and sea surface air pressures (in the range of 66.8–73.9%) on Buoys 44065,

Table 2
Comparison Between Central Locations and Minimum Central Pressures of the Model-Simulated Hurricane for the Cases With and Without OML

Variables	With OML (Global-FVCOM)	With OML (Global-HYCOM)	No OML
The maximum deviation distance (km)	66.4	82.9	176.6
STD of distance difference (km)	17.6	15.6	59.3
The maximum pressure difference (hPa)	5.3	5.2	8.2
STD of pressure difference (hPa)	3.0	3.6	4.1

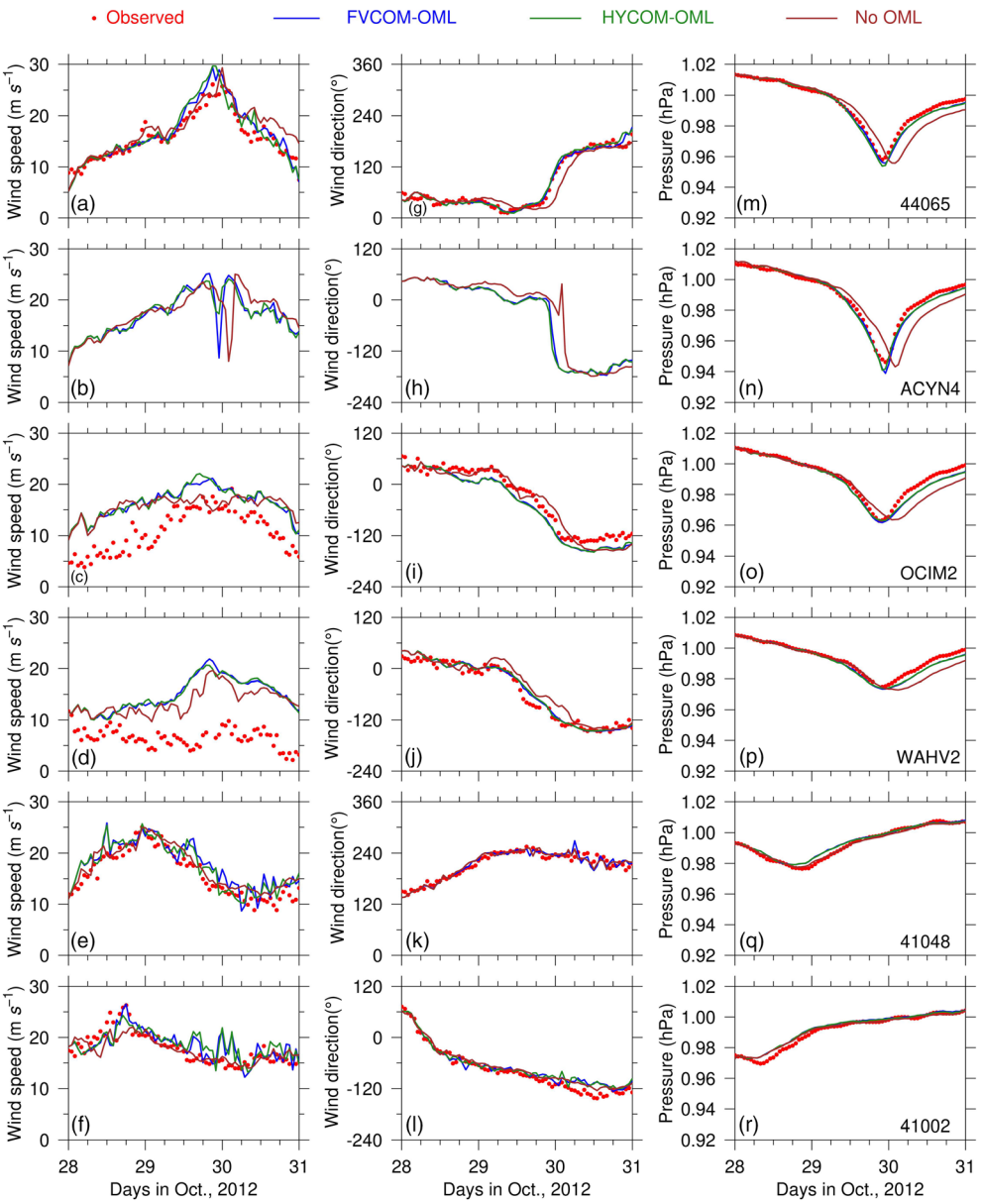

Figure 5. (a–r) Comparisons between simulated and observed 10-m wind speeds, 10-m wind directions, and sea level pressures at buoy stations 44065, ACYN4, OCIM2, WAHV2, 41048, and 41002 for the cases without and with the ocean mixed layer.

Table 3
Comparison Between the 10-m Wind and Sea Level Pressure Differences at Six Stations for the Cases With and Without OML

Stations	44065		ACYN4		OCIM2		WAHV2		41,048		41,002	
ΔWS_{max}	4.7	7.1	—	—	9.7	10.5	15.0	12.5	5.9	5.0	6.4	5.5
ΔWS_{STD}	1.7	2.1	—	—	2.3	3.3	3.6	2.8	2.0	1.4	2.3	1.9
ΔWD_{max}	30.8	60.6	—	—	39.0	41.0	28.9	47.2	38.0	27.2	38.1	24.5
ΔWD_{STD}	8.5	17.4	—	—	11.6	18.2	11.2	15.7	9.6	9.4	12.0	8.2
ΔSP_{max}	4.4	17.7	7.3	25.7	6.1	14.5	4.6	9.6	4.8	2.3	5.3	5.3
ΔSP_{STD}	1.8	6.8	2.3	8.6	1.9	5.8	1.5	4.0	1.6	1.0	1.5	1.8

Note. ΔWS_{max}: Maximum wind speed difference (m s^{-1}); ΔWS_{STD}: Standard deviation of the wind speed difference (m s^{-1}); ΔWD_{max}: Maximum wind direction difference (the degree to the north); ΔWD_{STD}: Standard deviation of the wind direction difference (the degree to the north); ΔSP_{max}: Maximum sea surface pressure difference (hPa); and ΔSP_{STD}: Standard deviation of the sea surface pressure difference (hPa). Shaded box: OML, Clear box: No OML. In this case, the initial OML was set up using the Global-FVCOM results.

ACYN4, and OCIM2, but not on WAHV2. At WAHV2, the standard deviation errors in simulated wind direction and sea air pressure were dropped by 28.8% and 62.8% after the OML was included, but the standard deviation errors in the wind speed were enlarged by 28.8%. WAHV2 was about 228.8 km left from the hurricane center when Hurricane Sandy made landfall, far away from the radius of the hurricane maximum wind speed. This result suggested that implementing the OML dynamics into the WRF could significantly improve the model performance to capture the wind and air pressure at and near the hurricane center but does not work in the surrounding region outside the strong wind area of the hurricane. It was not surprising to see little difference found initially between cases with and without OML, since the OML conditions were similar between these cases during the initial simulation period. When the hurricane moved onto the shelf, the OML depth significantly varied with time and in space, resulting in a rapid adjustment to the atmospheric environment. It was the reason why the model-data comparison was improved considerably on the nearshore buoys than on the open ocean buoys.

We also repeated all the experiments with the OML parameterizations produced by the Global-HYCOM and summarized statistical error analysis results in Table 4. Although distributions of h_m and $\overline{T}_{oml}$ obtained from the Global-HYCOM slightly differed from those obtained from the Global-FVCOM, the model-simulated pathways, wind speeds, wind directions, and sea surface air pressures of Hurricane Sandy with the OML from these two models remained the same level of overall accuracy.

Table 4
Performance Evaluation of the WRF Model With OML for the Cases of the Global-FVCOM and Global-HYCOM

	44065		ACYN4		OCIM2		WAHV2		41048		41002	
Stations	Diff	%	Diff	%	Diff	%	Diff	%	Diff	%	Diff	%
Global-FVCOM												
ΔWS_{max}	2.4	33.2	—	—	0.8	7.3	−2.5	−20.1	−0.9	−17.4	−0.9	−16.9
ΔWS_{STD}	0.4	17.5	—	—	1.0	30.1	−0.8	−26.8	−0.6	−40.1	−0.4	−23.4
ΔWD_{max}	29.8	49.1	—	—	1.9	4.7	18.4	38.9	−10.9	−40.1	−13.6	−55.3
ΔWD_{STD}	9.0	51.4	—	—	6.6	36.2	4.5	28.8	−0.2	−2.4	−0.3.7	−45.2
ΔSP_{max}	13.3	75.4	18.4	71.7	8.4	57.9	5.0	52.0	−2.6	−112.3	−0.1	−1.0
ΔSP_{STD}	5.0	73.9	6.3	73.0	3.9	66.8	2.5	62.8	−0.6	−52.8	0.3	14.9
Global-HYCOM												
ΔWS_{max}	1.4	19.9	—	—	0.7	7.1	−2.7	−21.7	−0.4	−7.8	−1.2	−21.7
ΔWS_{STD}	0.0	2.3	—	—	1.0	31.2	−0.7	−25.7	−0.4	−29.8	−0.5	−27.6
ΔWD_{max}	26.2	43.3	—	—	5.1	12.5	15.1	31.9	4.6	16.8	−15.2	−61.9
ΔWD_{STD}	8.1	46.5	—	—	6.3	34.5	4.5	28.4	−0.1	−0.6	−3.6	−43.2
ΔSP_{max}	12.5	70.4	18.6	72.5	8.7	59.9	5.2	54.5	−2.5	−109.2	0.0	−0.2
ΔSP_{STD}	5.0	72.8	6.3	73.9	3.9	66.6	2.5	63.3	−0.5	−52.0	0.2	11.8

Note. ΔWS_{max}: Maximum wind speed difference (m s^{-1}); ΔWS_{STD}: Standard deviation of the wind speed difference (m s^{-1}); ΔWD_{max}: Maximum wind direction difference (the degree to the north); ΔWD_{STD}: Standard deviation of the wind direction difference (the degree to the north); ΔSP_{max}: Maximum sea surface pressure difference (hPa); and ΔSP_{STD}: Standard deviation of the sea surface pressure difference (hPa). The symbol "Diff" is defined herein as the error difference between two cases without and with OML.

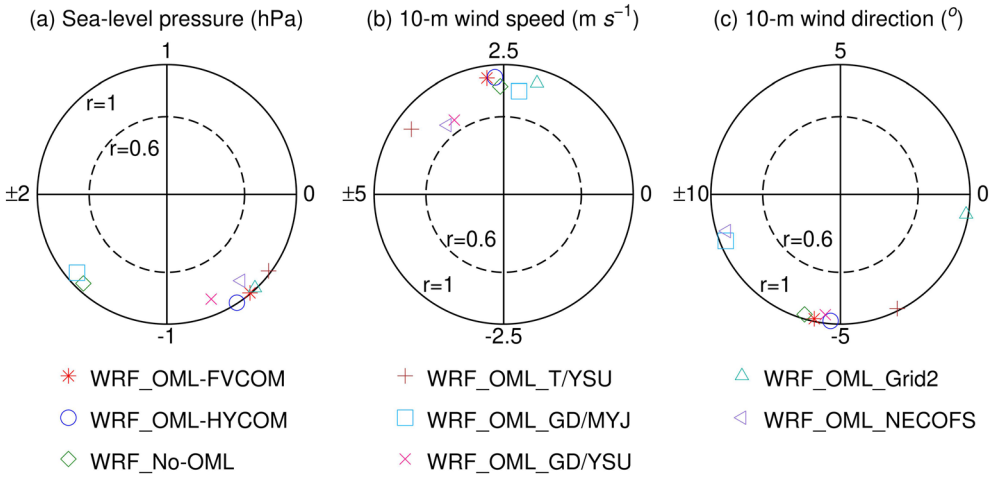

Figure 6. (a–c) Taylor diagrams summarizing the comparison results for the cases with and without OML, different parameterization schemes, and Grid-2 and NECOFS grid.

Taylor diagrams summarized the model-data comparison results for air pressures, wind speeds, and directions (Figure 6). Considering the statistics estimated from the comparison on six buoys, the WRF runs remained the same correlation level of >0.9 for air pressure and winds no matter if OML included or not. The significant difference was in the root-mean-square error (RMSE) of air pressure, which was 0.55 and 0.63 for the OML cases with an initial field of the Global-FVCOM and HYCOM, respectively, but up to 1.48 for the case with no OML.

3.2. OML Dynamics Attributing to Hurricane Sandy

In WRF, the sea level pressure is a function of air temperature, density, and vapor mixing ratio at the air-sea interface that is calculated by formula (Skamarock et al., 2008) given as

$$p = p_0 \left[\frac{r_d T_{air} \left(1 + \frac{r_v}{r_d} Q_{vapor}\right)}{p_0 \alpha_d} \right]^{\gamma} \quad (1)$$

where p is the sea level pressure, T_{air} is the air temperature, Q_{vapor} is the vapor mixing ratio, α_d is the dry gas inverse density, p_o is the reference pressure (set as 1,000 hPa), r_d and r_v are the gas constant for dry and moist airs, respectively, and γ is the heat capacity for dry air. To examine how the OML influences the simulated air pressure and wind fields, we compared the pressure-related variables (T_{air}, Q_{vapor}, α_d, and p) at hurricane locations on similar isobaths for the cases with and without OML. In the case without OML, the WRF-simulated hurricane moved slowly when compared with an observed storm, with a 3-h time delay for landfall. The comparison was made by selecting 1900 UTC 29 October and 2100 UTC 29 October for the cases with and without OML, respectively.

Although both cases were capable of capturing the typical hurricane features: high air temperature, moisture, and inverse density centralized cores and low central sea level pressure, their spatial scales for the OML case shrank toward the center (Figure 7). At the hurricane center, T_{air}, Q_{vapor}, and α_d all showed lower values when the OML dynamics were taken into account; they were 2.55°C, 1.2×10^{-2}, and 0.01 $m^3\ kg^{-1}$ lower, respectively. According to Equation 1, p was proportional positively to T_{air} and Q_{vapor} but inversely to α_d. In this case, p showed a drop of 11.14 or 5.20 hPa if only either T_{air} or Q_{vapor} was accounted for and a rise of 9.80 hPa if α_d was considered. The resulting central sea level pressure dropped to 939.16 hPa, which was 6.60 hPa lower than that in the case without OML.

Correspondingly, the maximum wind speed at the radius of maximum wind (R_{max}) increased to 37.30 m s^{-1} in the OML case, which was about 2.7 m s^{-1} stronger than that found in the case without OML. The comparison of the hurricane wind distribution for the two cases clearly showed that R_{max} decreased

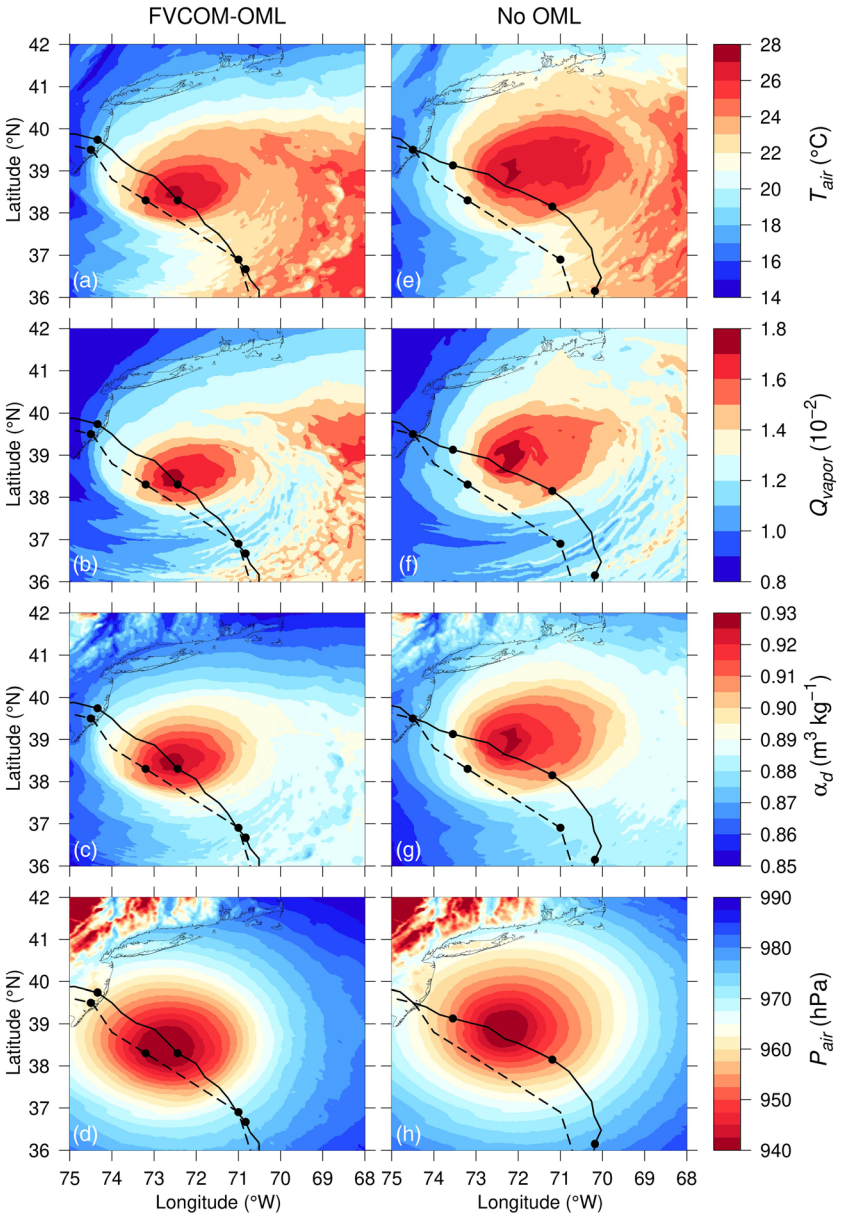

Figure 7. (a–h) Comparisons of air temperature (T_{air}), vapor ratio (Q_{vapor}), inverse density (α_d), and sea level pressure (p) for the cases with and without OML, at 1900 UTC 29 October and 2200 UTC 29 October, separately. The left columns are for the case with OML, and the right columns are for the case without OML. The black dashed line is the observed hurricane track, and the solid black line is the simulated hurricane track.

considerably when the OML dynamics activated (Figures 8a–8d). Since the WRF-simulated hurricane swirl did not follow a perfectly circular motion, the angular momentum was not conservative. After the OML was turned on, R_{max} was reduced from 184.41 to 134.90 km, while the maximum wind speed increased from 34.61 to 37.30 m s^{-1}. If it was a perfect circle rotating storm following the angular momentum conservation, the maximum wind speed at R_{max} should be up to 47.31 m s^{-1}, about 10 m s^{-1} stronger than the WRF-simulated maximum wind speed.

In the case without OML, the SST decreased toward the coast, with the temperature contours distributing approximately along isobaths (Figure 8f). In the case with OML, storm-induced mixing formed a colder SST zone in the inner shelf region, which significantly enhanced the cross- and along-isobath gradients of sea temperature not only beneath hurricane but also in the surrounding water (Figure 8e). At the

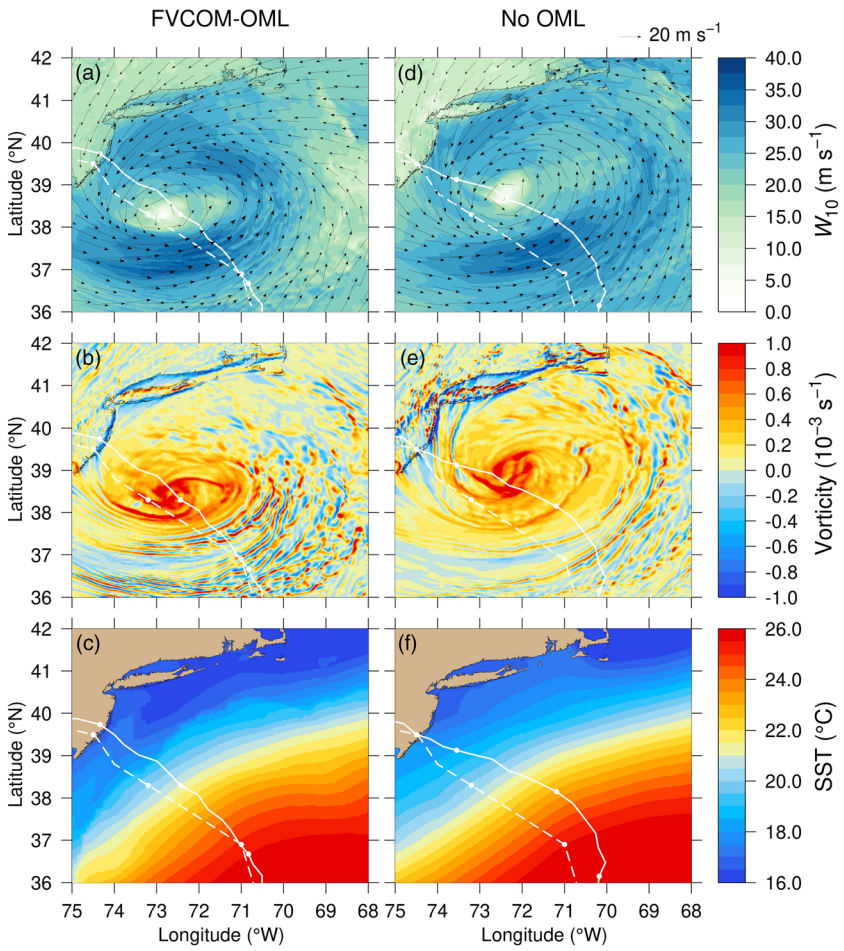

Figure 8. Comparisons of the 10-m wind speed (a, d), vorticity (b, e), and SST (c, f) for the cases with (left column) and without OML (right column). The white dash line is the observed hurricane track, and the solid white line is the simulated hurricane track.

maximum wind region, SST was ~2°C lower in the case with OML than in the case without OML. It implies that the air-sea interaction change was more active in the nearshore region than in the open water region. Because the SST varied considerably in space in the inner shelf region and also for a given time, the hurricane centers were at different locations in two cases with and without OML, the hurricane center may not be the right location to make a comparison between these two cases. Although the landfall times were different in these two cases, their landfall locations were closed to each other. To quantify the OML influences, a fixed site (shown in Figure 4 as a black triangle) was selected to make the comparison. There were two reasons to choose this location for the time series analysis. First, this was a site where the maximum wind zones of simulated hurricanes in both cases passed through. Second, the distances relative to the hurricane center in the two cases were the same, which allowed us to make an apple to apple comparison. We also tried to compare the two cases by selecting a fixed location in the open ocean. Since the trajectories of WRF-simulated hurricanes significantly differed in the open sea, however, it was impossible to find a site that could represent the maximum wind zone for both cases. The contribution of OML to the change of hurricane intensity can be viewed from the time series of the heat flux, air temperature, and sea temperature at the air-sea interface at this fixed site, where Hurricane Sandy passed by during the period from 0000 UTC 28 October to 2100 UTC 29 October (Figure 9).

For the case without the OML, when the local wind speed increased as the simulated hurricane came close (Figure 9a), the SST remained unchanged before and after the simulated storm passed, since no oceanic feedback was considered (Figure 9b). T_{air} decreased by ~3.0°C during a 24-h period since 1700 UTC 28 October, rose by ~2.0°C during a 3-h period around 1800 UTC 29 October, and then rapidly dropped again as the

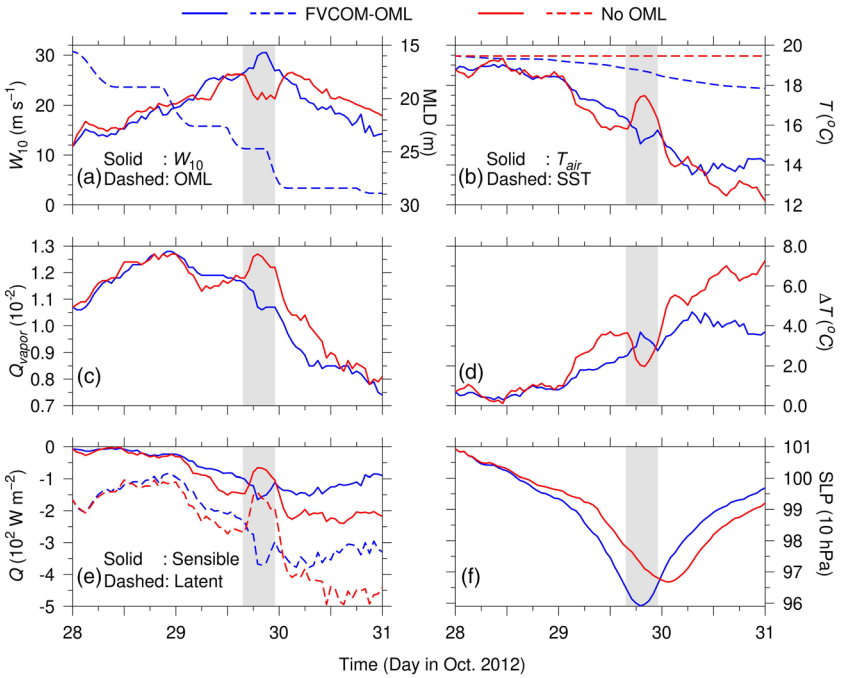

Figure 9. Time series of the 10-m wind speed (solid lines in a) and mixed layer depth (dashed line in a), 2-m air temperature (solid lines in b) and sea surface temperature (dashed lines in b), vapor ratio (c), sea air temperature difference (d), latent heat flux (dashed lines in e) and sensible heat flux (solid lines in e), and sea level pressure (f) at a selected location (shown in Figure 7) over the period from 0000 UTC 28 October to 2100 UTC 31 October. The results of the case with OML are shown in blue and the case without OML in red.

center of the simulated hurricane passed (Figure 9b). Corresponding to the T_{air} rise, the wind speed exhibited a drop from 26.1 to 21.2 m s^{-1} (Figure 9a); Q_{vapor} increased by 1.9×10^{-3} (Figure 9c). As a result, the latent and sensible losses from the ocean to the air reduced by ~130 and ~80 W m^{-2}, respectively (Figure 9e). The sea level pressure reached its minimum of 966.8 hPa at 0100 UTC 30 October (Figure 9f), about a 3-h delay than the observed hurricane.

For the case with the OML, at 0000 UTC 28 October, the local wind speed was ~12.0 m s^{-1} and then rapidly increased to ~31.0 m s^{-1} over a 43-h period as the hurricane passed (Figure 9a). The increase of wind-induced mixing caused a13.4-m deepening of the OML from 15.6 to ~29.0 m over 2 days from 0000 UTC 28 October to 0000 UTC 30 October and then remained the same level over 1 day after the hurricane passed (Figure 9a). As a result, the mean sea temperature of the OML dropped from 19.5°C to 18.7°C (Figure 9b). Over that period, the ocean remained warmer, whereas T_{air} decreased monotonously as the simulated hurricane moved close to the monitoring site (Figure 9b).

In the case without the OML, instead of the T_{air} rise, T_{air} rapidly dropped by ~1.4°C over the same period (Figure 9b), co-occurred with a drop of by 1.1×10^{-3} in Q_{vapor} (Figure 9c). This process produced an air-sea temperature difference peak of 3.7°C around the time when the maximum wind reached (Figure 9d), which was 1.7°C higher than that in the case without the OML. The latent and sensible heat losses from the ocean to the air were thus increased to 370.8 and 165.5 W m^{-2}, respectively (Figure 9e), which were about 228.1 and 99.5 W m^{-2} larger than those in the case without the OML. The minimum sea level pressure concurred with the appearances of peak air-sea temperature difference, latent/sensible heat flux, and the maximum wind. It was 959.1 hPa, occurring at 1900 UTC 29 October (Figure 9f), the time closed to the observed hurricane. The minimum sea level pressure was 7.7 hPa lower in the case with the OML than in the case without the OML.

The sections across the hurricane center were selected to compare the air temperatures and water vapor ratios for the cases with and without the OML (see the locations of the sections in Figure 4). To make an apple to apple comparison, we selected 1400 UTC 29 October for the case with OML and 1600 UTC 29 October for the case without OML, the times at which the WRF-simulated hurricanes crossed the sections

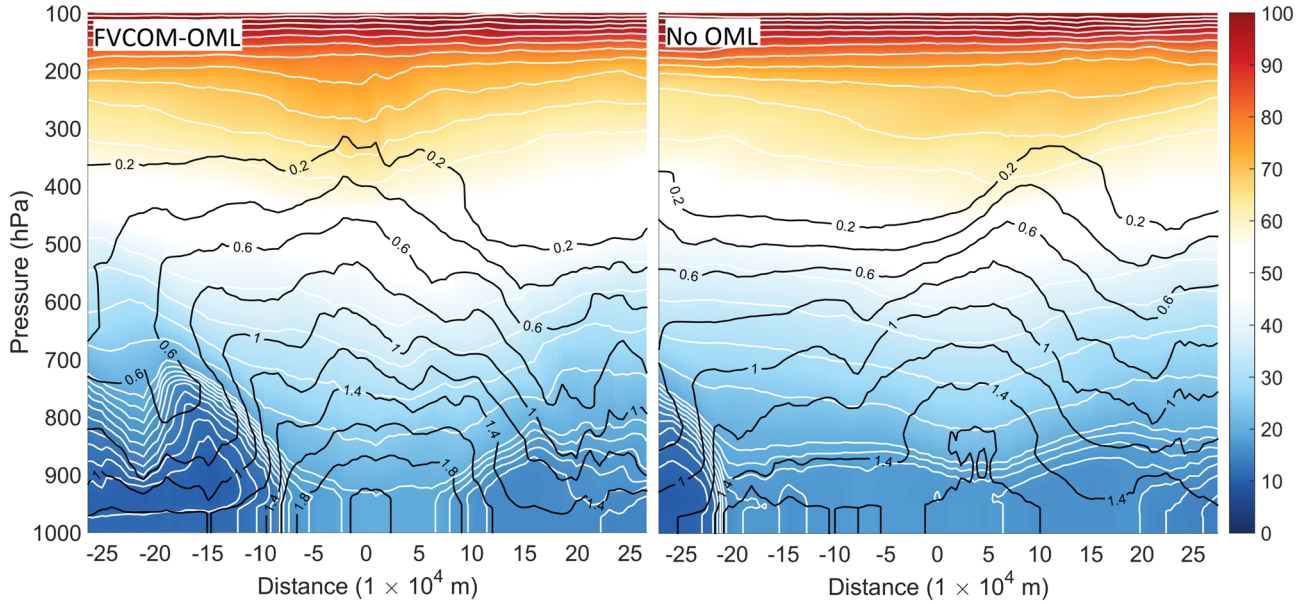

Figure 10. Distributions of the air temperature and water vapor ratio on the selected section across the hurricane center for the cases with and without the OML. The black lines are the isolines of the water vapor ratio. The white lines and images show the air temperature.

with their maximum wind zones closest to each other. The sections were perpendicular to the moving directions of the hurricane. For the two cases, the distribution patterns were the same, but the intensity and gradients significantly differed (Figure 10). As the OML was considered, the storm size shrank with the decrease of the max-wind radius. The max-wind zone was ~150 km away from the hurricane center, where the air temperature near the air-sea interface reached 11°C, ~9°C lower than that at the hurricane center. It was caused by cooling at the sea surface due to oceanic mixing. Besides, the water vapor ratio was decreased as altitude increased, with a maximum of ~2.0 near the sea surface around the hurricane center.

In contrast, in the case without the OML, the max-wind zone was ~250 km away from the hurricane center. At the lower level, the air temperature was 13.8°C within the max-wind area, which was about 1.7°C higher than that in the case with the OML. Besides, the water vapor ratio around the hurricane center was ~0.4 smaller than that in the case with the OML. The comparison results implied that ignoring the OML could lead to an underestimation of air temperature cooling in the maximum wind zone and water vapor ratio near the hurricane center and thus energy flux from the ocean to the hurricane.

As the same as previous hurricane measurements, in both the cases, the oceanic heat loss was predominated by the latent heat flux. The latent heat flux was one order of magnitude larger than the sensible heat flux. This result was consistent with the change of the latent heat flux in Hurricane Felix observed on the southern Georges Bank by Beardsley et al. (2003). The significant loss of latent and sensible oceanic heat flux transferred heat energy to a hurricane like a Carnot heat engine (Emanuel, 2003), which caused the air temperature to decrease rapidly. In the case with the OML, during Hurricane Sandy's passing period (the period shaded in Figure 9), intense wind-induced mixing made the atmosphere boundary cooler. Although this period was relatively shorter due to the faster moving speed of the hurricane, the sudden enlargement of both latent and sensible heat fluxes from the ocean to the atmosphere provided significant heat energy to the hurricane. This enhanced energy transfer directly cooled air temperature in the bottom layer above the sea surface and enlarged the sea-air temperature difference. The drop in sea surface air temperature and water vapor ratio directly resulted in a decrease in the central sea level pressure based on Equation 1 and strengthened the hurricane intensity. This finding was consistent with the diagnostic model results by Schade and Emanuel (1999). They found that decrease of the water vapor mixing ratio in the atmospheric near-surface boundary layer could positively affect the storm intensity.

In general, the OML-induced cooling of SST tended to weaken the heat loss from the ocean to the atmosphere (Figure 9e). Our model results indicated that the OML-produced cold wake underneath the storm

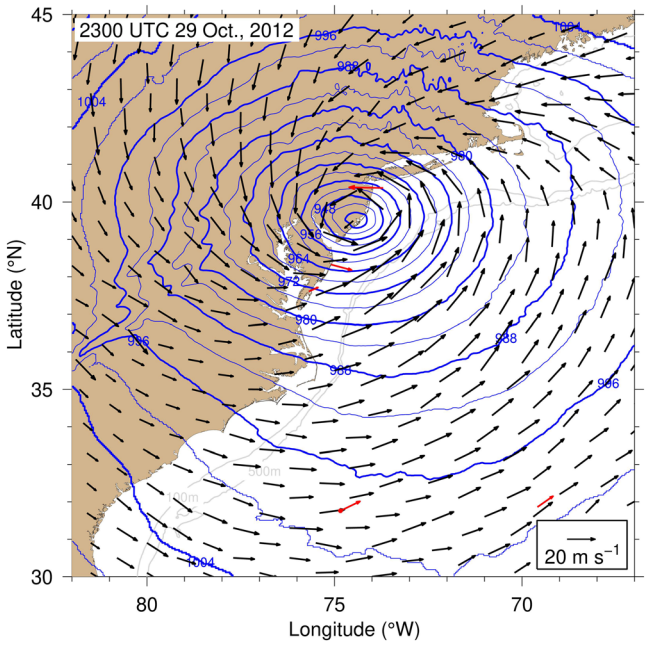

Figure 11. A snapshot of the distributions of the simulated wind vector (black color) and sea surface air pressure (blue color) of Hurricane Sandy overlapped by observed 10-m wind vectors (red color vectors) on the meteorological buoy stations at 2300 UTC 29 October 2012.

could lead to a large air-sea temperature difference at the maximum wind zone and a significant latent heat loss from the ocean within the storm, as well as rapid drops of the air temperature and vapor mixing ratio at the sea surface. This process directly strengthened the hurricane intensity and hence its pathway. Schade and Emanuel (1999) (S&E) examined the influence of SST on storm intensity through diagnostic model experiments by specifying different SST values in the model. In their cases, the SST remained unchanged with time and in space during the entire simulation period. Their works were to examine how a storm behaves under different background SST conditions. They found that the central sea level pressure increased by 6 hPa as SST decreased 1 K. This result suggested that colder background SST could have negative feedback on storm intensity. Bender et al. (1993) pointed out that the OML could positively or negatively impact the hurricane intensity. Our key findings are that including the OML dynamics produces a time-varying and spatially varying vertical mixing, causing a significant change of SST and thus heat flux exchanges between the ocean and atmosphere beneath a hurricane. As Hurricane Sandy moved toward the coast, intense vertical mixing brought cold water from the deep stratified layer toward the mixed layer to produce a cold wake within the storm, especially at the maximum wind zone. Since the hurricane-induced wind and air temperature significantly varied in space, the oceanic feedback to the atmosphere was not uniform within the hurricane. Rapid cooling of SST caused significant drops of the air temperature and vapor mixing ratio, increased the air-sea temperature difference, and produced a considerable amount of latent heat flux from the ocean to the storm. Since the feedback varied with wind intensity in and out of the storm, the hurricane was intensified as the central air pressure dropped. Improving air pressure simulation with the OML tended to shrink the storm size and thus strengthened the wind intensity, which provided a better simulation of hurricane pathway and landfall.

The comparison between the cases with and without the OML suggested that ignoring OML could either exclude or weaken the contribution of the wind-induced oceanic mixing to the heat flux from the ocean to the hurricane. Improving the air pressure simulation reduced not only the errors of the maximum wind speed but also those of wind direction. In the previous experiences for WRF applications, the model generally underestimated the intensity of a hurricane or extratropical storm due to the failure of reproducing the minimum central pressure. To make the WRF work for the storm simulation, one usually assimilated the observed air pressure record at the center into the model to strengthen the storm intensity or built an initial condition with a well-defined vortex structure based on observations via variational bogus data assimilation. These approaches generally worked well for the hindcast application, but not for the forecast operation. This study agreed with the previous works for other hurricanes in extratropical regions (Sun et al., 2013), supporting the OML dynamics' addition to the WRF.

4. Discussion and Conclusions

The WRF model experiments were made to examine the influences of OML on intensity, pathway, and landfall of October 2012 Hurricane Sandy. The OML fields used in the experiments were from the real-time simulated field produced by the Global-FVCOM and Global-HYCOM. Comparing the model results for the cases with and without the OML showed that including the OML parameterization could significantly improve the accuracy of the hurricane pathway and intensity of the minimum central pressure.

When a hurricane moved toward the coast above the ocean, intense wind mixing deepened the surface mixed layer. Rapid cooling of SST and increase of water vapor ratio enhanced the latent and sensible heat loss from the ocean to the hurricane. The OML-induced oceanic heat loss was predominated by the latent heat flux, with one order of magnitude larger than the sensible heat flux. The significant loss of latent and

sensible oceanic heat fluxes transferred energy to a hurricane like a Carnot heat engine, causing the air temperature and water vapor ratio to decrease and increase rapidly, respectively. These processes led to a drop in the minimum central pressure and intensification of the hurricane intensity. Ignoring OML dynamics in the WRF hurricane simulation could either excluded or weakened the contribution of the wind-induced oceanic mixing to the heat flux from the ocean to hurricane and hence caused a significant bias.

In addition to the OML, the PBL and cumulus parameterizations need to be chosen with caution, particularly for the cumulus scheme (see Appendix A). The WRF performed better with the MYJ/Tiedtke parameterization than with the YSU/Tiedtke, YSU/G-D, and MYJ/G-D parameterizations. The simulation results were also sensitive to the design and grid resolution of the two-way nested grid. The domain covering the southern region of the early development stage of the hurricane and grid refinement in the coastal area provided better simulation results of hurricane center pathway, timing, and intensity.

It should be pointed out here that the WRF still showed an issue capturing the asymmetric spatial distribution of the hurricane-induced wind field. The model-data comparison made on coastal meteorological buoys showed a better agreement on the right side of the hurricane center than on the left side of the hurricane center. An example of evidence was shown in Figure 11: snapshots of the distribution of the wind vector (blue color) and sea level pressure were taken at 2300 UTC 29 October. At that time, Hurricane Sandy was very close to the coast for landfall. The simulated hurricane featured a symmetric wind field, while the observed wind was distributed asymmetrically to the hurricane center, stronger on the right side than on the left side. It was clear that the overestimation of the wind speed on the left side was due to a failure of the WRF to capture the asymmetric wind distribution structure of Hurricane Sandy.

Sun et al. (2013) used the current-wave interaction FVCOM to simulate Hurricane Bob induced storm surge on the U.S. northeast coast. Hurricane Bob made landfall near Newport, Rhode Island, around 1800 UTC 19 August 1991. When this hurricane moved northeastward over the continental shelf, it featured a core of maximum significant wave height on its right side. The current-wave interaction was more energetic on the right side than on the left side, which could directly contribute to the asymmetric structure of Hurricane Bob's wind field. To capture the asymmetric structure of the wind field of Hurricane Bob, they had to use the combined wind and air pressure from a hurricane model and WRF (Avila & Pasch, 1992; Bretschneider, 1972; Houston et al., 1999; Jelesnianski, 1966; Phadke et al., 2003; Powell & Black, 1990). Sun et al. (2013) studies also suggested that the current-wave interaction is directly attributed to the asymmetric distributions of the hurricane-driven oceanic current and water temperature.

Our experiments highlighted the roles of the OML in capturing the intensity and movement of Hurricane Sandy. This result implies the importance of the air-sea interaction in the hurricane simulation. The asymmetric issue described above can be addressed using a coupled WRF and ocean model. The fully coupled WRF and FVCOM model has been developed on the framework of the ESMF (Earth System Modeling Framework), with the implementation of nonhydrostatic air-sea and current-wave interaction processes. In the coupled model, the WRF model transfers the atmospheric fields of sea surface wind, heat fluxes, evaporation, and precipitation to FVCOM. Meanwhile, WRF bottom boundary is provided every time step with SST, significant wave height, wavelength, and wave period predicted by FVCOM. Further experiments with this coupled model are being conducted to address the unsolved issues and problems raised from this study.

Appendix A: Sensitivity of WRF Simulations to Parameterizations and Grid Settings

The PBL parameterization can affect not only the intensification of storms and hurricanes (Braun & Tao, 2000; Karyampudi et al., 1998; Kepert, 2012; Li & Pu, 2008) but also the air-sea heat flux. Braun and Tao (2000) examined how a mesoscale meteorological model performed under nine different PBL parameterization schemes. They found that the difference in MSLP could be up to 16 hPa. A similar finding was reported for the 2005 Hurricane Emily by Li and Pu (2008), who found that an MSLP difference produced by two boundary layer parameterization schemes could reach 19 hPa. C. Chen et al. (2005) assessed the impacts of different PBL parameterization schemes on sensible and latent heat fluxes, reporting that during storm events, the mean absolute difference and standard deviation between model-simulated and observed sea surface heat fluxes among those schemes could be up to ~140–150 W m^{-2} for latent flux and

~180–200 W m^{-2} for sensible flux, respectively. These errors were about 1 or 2 times larger than observed fluxes.

It is debatable whether horizontal grid resolution significantly influences the WRF simulation (Fierro et al., 2009; Marks & Shay, 1998). The WRF is generally operated using multidomain nesting grids, with the option of refining the grid over the storm- or hurricane-influenced area (S. S. Chen et al., 2007; Gopalakrishnan et al., 2006; Warner, 2011). The grid refinement can be automatically done when the storm vortex is well defined at a specific pressure surface (either 500 or 850 hPa). Although some experiments showed that increasing the horizontal grid resolution can improve the storm simulation results (Marks & Shay, 1998), it was not always accurate in other cases. For example, Fierro et al. (2009) storm simulation results suggested that both maximum wind speed and MSLP changed little as the horizontal grid resolution was refined from 5 to 1 km. It seems like refining the grid over the sea surface could only help reduce the numerical truncation error if the ocean boundary condition was specified with a scale larger than the model resolution.

Built on the WRF with OML dynamics, we also examined the influence of the combination of cumulus and PBL schemes on the intensity and pathway of Hurricane Sandy. In this study, the Tiedtke (Tiedtke, 1989) and Grell-Devenyi (G-D) ensemble schemes (Grell & Dévényi, 2002) were selected for the cumulus parameterization, and Mellor-Yamada-Janjić (MYJ) (Janjić, 1994) and Yonsei University (YSU) (Hong et al., 2006) schemes were for the PBL parameterization. The simulation was re-run for three additional cases with (a) Tiedtke and YSU, (b) G-D ensemble and MYJ schemes, and (c) G-D ensemble and YSU. The results were compared with the default setup case shown in Table 1.

The sensitivity studies of the impact of domain setting on the accuracy and reality of WRF-simulated Hurricane Sandy were conducted by running the WRF with two different configurations of the computational domain shown in Figures 2b and 2c. Grid-2 is similar to Grid-1 used in the default setup listed in Table 1 and Figure 2a. Both consist of three two-way nesting domains with grid resolutions of 27, 9, and 3 km, respectively. The only difference was that D-3 in Grid 2 was centered in the Mid-Atlantic Bight region, with its southern boundary extending to ~30°N and eastern boundary shifting westward to ~65°W. Grid-3 consisted of only two domains with the southernmost boundary around 32°N. The horizontal grid resolutions of these two domains are 27 and 9 km, respectively, which were the same as D-1 and D-2 in Grid-1 and Grid-2. It is the WRF grid used for the Northeast Coastal Ocean Forecast System (NECOFS), which is supported by the NOAA-IOOS-funded Northeastern Regional Association of Coastal Ocean Observing Systems (NERACOOS). NECOFS was placed into the 24/7 forecast and hindcast operations since 2007 (Beardsley et al., 2013; C. Chen et al., 2013). The comparison of the results produced by Grid-1 and Grid-2 provided insights into the model performance for given domain configurations under the same horizontal grid resolutions. The comparisons made for Grid-1 and Grid-3 results were made to evaluate the performance of NECOFS in the tropical storm forecast operation.

The simulation experiments showed that besides the influence of OML, the WRF hurricane simulation results were also sensitive to PBL and cumulus parameterization schemes, domain setup, and horizontal grid resolution. For both the cases without and with the OML, we found that the combination of the MYJ scheme for PBL and the Tiedtke scheme for cumulus parameterization provided us with better overall simulation results (Figures 4, A1a, and A1b). Changing the MYJ scheme to the YSU scheme while retaining the same Tiedtke cumulus scheme, we found that the simulation error became larger in both the hurricane path's deviation distance and the minimum central pressure. The hurricane path's distance errors were increased by 18.6 km for the standard deviation distance and 8.0 km for the standard deviation. The minimum central pressure error was also up by 2.6 hPa for its maximum difference value and 1.4 hPa for its standard deviation. The situation became much worse when the cumulus scheme was changed. For the case with the MYJ/G-D scheme, the distance errors for the hurricane path were increased by 129.0 km for the maximum deviation distance and 49.4 km for the standard deviation error of distance difference, respectively. For the case with the YSU/G-D scheme, these errors were increased by 180.3 and 79.2 km, respectively. The cumulus scheme's influences on the minimum central pressure were not significant than those on the hurricane path. The increases in the maximum and standard deviation errors were 1.4 and 1.0 hPa for the case with the MYJ/G-D scheme and 1.1 and 0.5 hPa for the case with the YSU/G-D scheme.

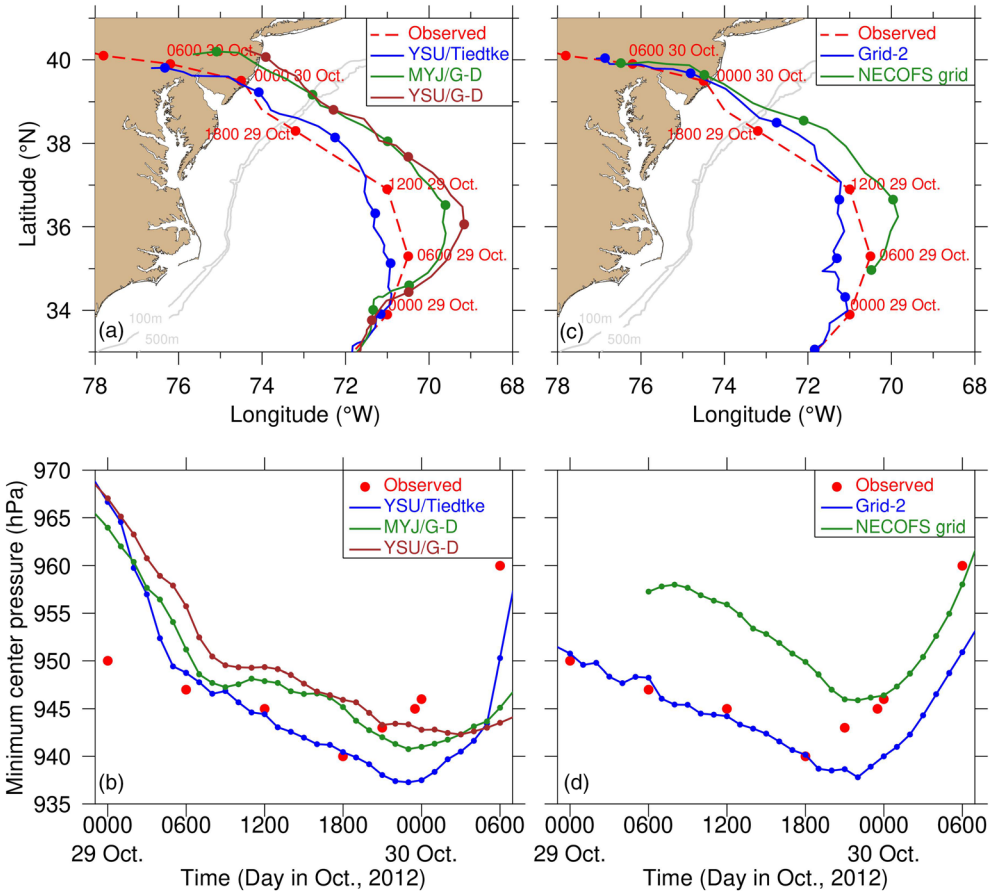

Figure A1. Comparisons between the simulated and observed pathways of Hurricane Sandy (a and c) and minimum central pressures (b and d) for the cases with the parameterization schemes YSU/Tiedtke, MYJ/G-D, and YSU/G-D (a and b) and using Grid-2 and NECOFS grid (c and). In all these cases, the OML was included. Labels shown in the upper panel are the time of year, month, day, hour, and minute. All the time and dates are in UTC.

We also assessed the model performance with the YSU PBL scheme and G-D cumulus scheme by comparing the simulated wind speed, wind direction, and sea level pressures with measurement records on buoy stations, with statistical error summaries in the Taylor diagram in Figure 6. Compared with the MYJ/Tiedtke parameterization, the primary error increase from the YSU/Tiedtke, MYJ/G-D, and YSU/G-D schemes appeared in the timing of the minimum central pressures when Hurricane Sandy made landfall. At stations 44065, ACYN4, OCIM2, and WAHV2, the simulated minimum sea level pressure timing was about a 4-to-6-h delay compared with observational records. Changing the MYJ/Tiedtke to the YSU/Tiedtke led to an increase in the RSME of wind speed from 2.73 to 4.02 m s^{-1}, with the RSMEs of sea level pressure and wind direction were lower. Selecting MYJ/G-D scheme enlarged the RSMEs of sea level pressure and wind direction from 0.55 to 1.55 hPa and from 5.66° to 8.78°, respectively, but the RSME of the wind speed was lower. Regarding an overall error, the YSU/G-D scheme showed the worst performance, with the RSME of 0.74 in sea level pressure, 3.43 m s^{-1} in wind speed, and 5.40° in wind direction.

The only difference between Grid-1 and Grid-2 was that the D-3 in the Grid-2 case extended further south, with the eastern boundary shifting eastward. Results showed that this difference did not significantly impact the overall statistical simulation accuracy of Hurricane Sandy's path and its center air pressure (Figures A1c and A1d). The Grid-3 case consisted of only two two-way nested domains. Although the D-2 domain in the Grid-3 case was the same as the D-3 domain in the Grid-1 case, the horizontal grid resolution in that D-2 domain was three times coarser. Also, the Grid-3 case did not cover the area where Hurricane Sandy originally developed in the tropical region. In this case, even when the model was configured with the calibrated initial field, the path of the simulated Hurricane Sandy deviated significantly eastward after 0600 UTC 29 October (Figure A1c). The maximum deviation distance error was about 166.4 km larger than that in the

Grid-1 case, even the standard deviation error for the path difference was 53.4 km larger. The model also failed to capture the minimum central pressure. The maximum and standard deviation errors of the minimum central pressure at the hurricane center were 19.9 and 5.7 hPa larger than those in the Grid-1 case. Similar results were found on the model-data comparison on buoys, with larger RSME in wind speed and direction when Grid-3 was used (Figure 6). We also conducted the experiments by adding D-3 in the Grid-3 case with the same grid resolution as the D-3 in the Grid-1 case, but the results were not significantly improved.

The comparison results between the Grid-3 and Grid-1 cases suggested that even when the OML was included, the domain and horizontal grid resolution setups were also critical. To capture the realistic path of Hurricane Sandy, one needs to set up the computational domain to cover the tropical region with the hurricane's early development stage. The Grid-3 case has the same domain configure used for the NECOFS. In the NECOFS operation, the WRF model was run with the data assimilation calibrated initial conditions by including all available meteorological buoy data. This assimilation approach helped reduce the hurricane forecast errors, but it was not enough to provide the same accuracy results, as shown in the Grid-1 case. An effort has been made to replace the current NECOFS WRF domain by the Grid-1 domain setup.

Data Availability Statement

All the data used in this paper can be downloaded from the link with an address (at http://www.smast.umassd.edu:8080/thredds/catalog/models/fvcom/NECOFS/Archive/catalog.html).

Acknowledgments

This work was supported by the MIT Sea Grant College Program through grant 2017-R/RCM-49C and 2012-R/RC-127, the NSF grants OCE1459096, OCE1332207, and OCE1332666, the NOAA-funded IOOS NERACOOS program for NECOFS with subcontract numbers NA16NOS0120023 and NERACOOS A002 and A007, and the NOAA-CINAR Hurricane Sandy fund. The development of the Global-FVCOM system has been supported by NSF grants OCE1603000. S. Li was supported partially by the oversea Ph.D. fellowship from the China Scholarship Council (No. 1409010025).

References

Avila, L. A., & Pasch, R. J. (1992). Atlantic hurricane season of 1991. *Monthly Weather Review*, *120*(11), 2688–2696. https://doi.org/10.1175/1520-0493(1992)120%3C2688:ATSO%3E2.0.CO;2

Beardsley, R. C., Chen, C., & Xu, Q. (2013). Coastal flooding in Scituate (MA): A FVCOM study of the 27 December 2010 nor'easter. *Journal of Geophysical Research: Oceans*, *118*, 6030–6045. https://doi.org/10.1002/2013JC008862

Beardsley, R. C., Lentz, S. J., Weller, R. A., Limeburner, R., Irish, J. D., & Edson, J. B. (2003). Surface forcing on the southern flank of Georges Bank, February–August 1995. *Journal of Geophysical Research*, *108*(C11), 8007. https://doi.org/10.1029/2002JC001359

Bender, M. A., Ginis, I., & Kurihara, Y. (1993). Numerical simulations of tropical cyclone-ocean interaction with a high-resolution coupled model. *Journal of Geophysical Research*, *98*, 23,245–23,263. https://doi.org/10.1029/93JD02370

Blake, E. S., Kimberlain, T. B., Berg, R. J., Cangialosi, J. P. & Beven, J. L. II (2013). Tropical cyclone report: Hurricane Sandy (AL182012) October 22–29, 2012, National Hurricane Center Rep., (p 157). https://www.nhc.noaa.gov/data/tcr/AL182012_Sandy.pdf

Braun, S. A., & Tao, W.-K. (2000). Sensitivity of high-resolution simulations of Hurricane Bob (1991) to planetary boundary layer parameterizations. *Monthly Weather Review*, *128*(12), 3941–3961. https://doi.org/10.1175/1520-0493(2000)129%3C3941:SOHRSO%3E2.0.CO;2

Bretschneider, C. L. (1972). A non-dimensional stationary hurricane wave model, *Proc. 1972 Offshore Technology Conf.*, Houston, TX, OTC, 30-42. https://doi.org/10.4043/1517-MS

Chen, C., Beardsley, R. C., Hu, S., Xu, Q., & Lin, H. (2005). Using MM5 to hindcast the ocean surface forcing fields over the Gulf of Maine and Georges Bank region. *Journal of Atmospheric and Oceanic Technology*, *22*(2), 131–145. https://doi.org/10.1175/JTECH-1682.1

Chen, C., Beardsley, R. C., Luettich, R. A. Jr., Westerink, J. J., Wang, H., Perrie, W., et al. (2013). Extratropical storm inundation testbed: Inter-model comparisons in Scituate, Massachusetts. *Journal of Geophysical Research: Oceans*, *118*, 5054–5073. https://doi.org/10.1002/jgrc.20397

Chen, C., Gao, G., Qi, J., Proshutinsky, A., Beardsley, R. C., Kowalik, Z., et al. (2009). A new high-resolution unstructured grid finite volume Arctic Ocean model (AO-FVCOM): An application for tidal studies. *Journal of Geophysical Research*, *114*, C08017. https://doi.org/10.1029/2008JC004941

Chen, C., Gao, G., Zhang, Y., Beardsley, R. C., Lai, Z., Qi, J., & Lin, H. (2016). Circulation in the Arctic Ocean: Results from a high-resolution coupled ice-sea nested Global-FVCOM and Arctic-FVCOM system. *Progress in Oceanography*, *141*, 60–80. https://doi.org/10.1016/j.pocean.2015.12.002

Chen, S. S., Price, J. F., Zhao, W., Donelan, M. A., & Walsh, E. J. (2007). The CBLAST-Hurricane program and the next-generation fully coupled atmosphere-wave-ocean models for hurricane research and prediction. *Bulletin of the American Meteorological Society*, *88*, 311–318. https://doi.org/10.1175/BAMS-88-3-311

Chen, S. S., Zhao, W., Donelan, M. A., & Tolman, H. L. (2013). Directional wind-wave coupling in fully coupled atmosphere-wave-ocean models: Results from CBLAST-Hurricane. *Journal of the Atmospheric Sciences*, *70*(10), 3198–3215. https://doi.org/10.1175/JAS-D-12-0157.1

Cione, J. J., & Uhlhorn, E. W. (2003). Sea surface temperature variability in hurricanes: Implications with respect to intensity change. *Monthly Weather Review*, *131*(8), 1783–1796. https://doi.org/10.1175//2562.1

Dare, R. A., & McBride, J. L. (2011). Sea surface temperature response to tropical cyclones. *Monthly Weather Review*, *139*(12), 3798–3808. https://doi.org/10.1175/MWR-D-10-05019.1

Davis, C., Wang, W., Chen, S. S., Chen, Y., Corbosiero, K., DeMaria, M., et al. (2008). Prediction of landfalling hurricanes with the Advanced Hurricane WRF model. *Monthly Weather Review*, *136*(6), 1990–2005. https://doi.org/10.1175/2007MWR2085.1

Diakakis, M., Deligiannakis, G., Katsetsiadou, K., & Lekkas, E. (2015). Hurricane Sandy mortality in the Caribbean and continental North America. *Disaster Prevention and Management*, *24*(1), 132–148. https://doi.org/10.1108/DPM-05-2014-0082

Dukhovskoy, D. S., Morey, S. L., & O'Brien, J. J. (2006). Influence of multi-step topography on barotropic waves and consequences for numerical modeling. *Ocean Model*, *14*(1–2), 45–60. https://doi.org/10.1016/j.ocemod.2006.03.002

Emanuel, K. (2003). Tropical cyclones. *Annual Review of Earth and Planetary Sciences*, *31*(1), 75–104. https://doi.org/10.1146/annurev.earth.31.100901.141259

Fierro, A. O., Rogers, R. F., Marks, F. D., & Nolan, D. S. (2009). The impact of horizontal grid spacing on the microphysical and kinematic structures of strong tropical cyclones simulated with the WRF-ARW model. *Monthly Weather Review*, *137*(11), 3717–3743. https://doi.org/10.1175/2009MWR2946.1

Gao, G., Chen, C., Qi, J., & Beardsley, R. C. (2011). An unstructured grid, finite-volume sea ice model: Development, validation, and application. *Journal of Geophysical Research*, *116*, C00D04. https://doi.org/10.1029/2010JC006688

Glenn, S. M., Miles, T. N., Seroka, G. N., Xu, Y., Forney, R. K., Yu, F., et al. (2016). Stratified coastal ocean interactions with tropical cyclones. *Nature Communications*, *7*(1), 10887. https://doi.org/10.1038/ncomms10887

Gopalakrishnan, S. G., Surgi, N., Tuleya, R., & Janjić, Z. (2006). 7A. 3: NCEP Two-way-Interactive-Moving-Nest NMM-WRF modeling system for Hurricane Forecasting, *27th Conference on Hurricanes and Tropical Meteorology, Monterey*, *CA*, *American Meteorological Society*, Ar. A. 7. http://ams.confex.com/ams/pdfpapers/107899.pdf

Grell, G. A., & Dévényi, D. (2002). A generalized approach to parameterizing convection combining ensemble and data assimilation techniques. *Geophysical Research Letters*, *29*(14), 1693. https://doi.org/10.1029/2002GL015311

Griffies, S. M., Adcroft, A., Böning, C. W., Chassignet, E. P., Curchitser, E., Danabasoglu, G., et al. (2009). Problems and prospects in large-scale ocean circulation models. *Proceedings of Ocean Obs*, *9*, 410–431.

Hong, S. Y., Noh, Y., & Dudhia, J. (2006). A new vertical diffusion package with an explicit treatment of entrainment processes. *Monthly Weather Review*, *134*(9), 2318–2341. https://doi.org/10.1175/MWR3199.1

Houston, S. H., Shaffer, W. A., Powell, M. D., & Chen, J. (1999). Comparisons of HRD and SLOSH surface wind fields in hurricanes: Implications for storm surge modeling. *Weather and Forecasting*, *14*, 671–686. https://doi.org/10.1175/1520-0434(1999)014<0671:COHASS>2.0.CO;2

Hurlburt, H. E., Brassington, G., Drillet, Y., Kamachi, M., Benkiran, M., Bourdallé-Badie, R., et al. (2009). High-resolution global and basin-scale ocean analyses and forecasts. *Oceanography*, *22*(3), 110–127. https://doi.org/10.5670/oceanog.2009.70

HYCOM.org (2013). HYCOM + NCODA global 1/12° analysis, GLBa0.08, HYCOM.org, accessed 24 January 2016. https://www.hycom.org/data/glba0pt08/expt-90pt9

Jacob, S. D., Shay, L. K., Mariano, A. J., & Black, P. G. (2000). The 3D oceanic mixed layer response to Hurricane Gilbert. *Journal of Physical Oceanography*, *30*(6), 1407–1429. https://doi.org/10.1175/1520-0485(2000)030<1407:TOMLRT>2.0.CO;2

Janjić, Z. I. (1994). The step-mountain eta coordinate model: Further developments of the convection, viscous sublayer, and turbulence closure schemes. *Monthly Weather Review*, *122*(5), 927–945. https://doi.org/10.1175/1520-0493(1994)122<0927:TSMECM>2.0.CO;2

Jelesnianski, C. P. (1966). Numerical computations of storm surges with bottom stress. *Monthly Weather Review*, *95*(11), 740–756. https://doi.org/10.1175/1520-0493(1967)095<0740:NCOSSW>2.3.CO;2

Karyampudi, V. M., Lai, G. S., & Manobianco, J. (1998). Impact of initial conditions, rainfall assimilation, and cumulus parameterization on simulations of Hurricane Florence. *Monthly Weather Review*, *126*(12), 3077–3101. https://doi.org/10.1175/1520-0493(1998)126<3077:IOICRA>2.0.CO;2

Kepert, J. D. (2012). Choosing a boundary layer parameterization for tropical cyclone modeling. *Monthly Weather Review*, *140*(5), 1427–1445. https://doi.org/10.1175/MWR-D-11-00217.1

Knapp, K. R., Kruk, M. C., Levinson, D. H., Diamond, H. J., & Neumann, C. J. (2010). The International Best Track Archive for Climate Stewardship (IBTrACS): Unifying tropical cyclone best track data. *Bulletin of the American Meteorological Society*, *91*(3), 363–376. https://doi.org/10.1175/2009BAMS2755.1

Lee, C.-Y., & Chen, S. S. (2014). Stable boundary layer and its impact on tropical cyclone structure in a coupled atmosphere-ocean model. *Monthly Weather Review*, *142*, 1927–1944. https://doi.org/10.1175/MWR-D-13-00122.1

Li, X., & Pu, Z. (2008). Sensitivity of numerical simulation of early rapid intensification of Hurricane Emily (2005) to cloud microphysical and planetary boundary layer parameterizations. *Monthly Weather Review*, *136*(12), 4819–4838. https://doi.org/10.1175/2008MWR2366.1

Lin, I.-I., Black, P., Price, J. F., Yang, C. Y., Chen, S. S., Lien, C. C., et al. (2013). An ocean coupling potential intensity index for tropical cyclones. *Geophysical Research Letters*, *40*, 1878–1882. https://doi.org/10.1002/grl.50091

Lin, I.-I., Pun, I.-F., & Wu, C. -C. (2009). Upper ocean thermal structure and the western North Pacific category-5 typhoons—Part II: Dependence on translation speed. *Monthly Weather Review*, *137*(11), 3744–3757. https://doi.org/10.1175/2009MWR2713.1

Lin, I.-I., Wu, C.-C., Emanuel, K. A., Lee, I. H., Wu, C. R., & Pun, I. F. (2005). The interaction of Supertyphoon Maemi (2003) with a warm ocean eddy. *Monthly Weather Review*, *133*(9), 2635–2649. https://doi.org/10.1175/MWR3005.1

Lin, I.-I., Wu, C.-C., Pun, I. F., & Ko, D. S. (2008). Upper-ocean thermal structure and the western North Pacific category-5 typhoons. Part I: Ocean features and category-5 typhoon intensification. *Monthly Weather Review*, *136*(9), 3288–3306. https://doi.org/10.1175/2008MWR2277.1

Marks, F. D., & Shay, L. K. (1998). Landfalling tropical cyclones: Forecast problems and associated research opportunities. *Bulletin of the American Meteorological Society*, *79*(2), 305–323.

MEDML (2013). The 35-year Global-FVCOM product, Marine Ecosystem Dynamics Modeling Lab, accessed 24 January 2016. http://134.88.228.119:8080/fvcomwms/.

Miles, T., Seroka, G., & Glenn, S. (2017). Coastal ocean circulation during Hurricane Sandy. *Journal of Geophysical Research: Oceans*, *122*, 7095–7114. https://doi.org/10.1002/2017JC013031

Mooney, P., Gill, D. O., Mulligan, F. J., & Bruyère, C. L. (2016). Hurricane simulation using different representations of atmosphere-ocean interaction: The case of Irene (2011). *Atmospheric Science Letters*, *17*(7), 415–421. https://doi.org/10.1002/asl.673

NDBC (1996). Historical NDBC data, National Data Buoy Center, accessed 21 March 2016. https://www.ndbc.noaa.gov/historical_data.shtml

NOAA/NCEP (2000). NCEP FNL operational model global tropospheric analyses, continuing from July 1999 (updated daily), NCAR computational and information systems laboratory research data archive, accessed 28–31 October 2012. https://doi.org/10.5065/D6M043C6

Phadke, A. C., Martino, C. D., Cheung, K. F., & Houston, S. H. (2003). Modeling of tropical cyclone winds and waves for emergency management. *Ocean Engineering*, *30*(4), 553–578. https://doi.org/10.1016/S0029-8018(02)00033-1

Pollard, R. T., Rhines, P. B., & Thompson, R. O. (1972). The deepening of the wind-mixed layer. *Geophysical and Astrophysical Fluid Dynamics*, *4*(4), 381–404. https://doi.org/10.1080/03091927208236105

Powell, M. D., & Black, P. G. (1990). The relationship of hurricane reconnaissance flight-level wind measurements to winds measured by NOAA oceanic platforms. *Journal of Wind Engineering and Industrial Aerodynamics*, *36*, 381–392. https://doi.org/10.1016/0167-6105(90)90322-4

Price, J. F. (2009). Metrics of hurricane-ocean interaction: Vertically-integrated or vertically-averaged ocean temperature? *Ocean Science*, *5*(3), 351–368. https://doi.org/10.5194/os-5-351-2009

Schade, L. R., & Emanuel, K. A. (1999). The ocean effect on the intensity of tropical cyclones: Results from a simple coupled atmosphere-ocean model. *Journal of the Atmospheric Sciences*, *56*(4), 642–651. https://doi.org/10.1175/1520-0469(1999)056<0642:TOSEOT>2.0.CO;2

Shin, J. H., & Zhang, D. (2017). The impact of moist frontogenesis and tropopause undulation on the intensity, size, and structural changes of Hurricane Sandy (2012). *Journal of the Atmospheric Sciences*, *74*, 893–913. https://doi.org/10.1175/JAS-D-15-0362.1

Skamarock, W. C., Klemp, J. B., Dudhia, J., Gill, D. O., Barker, D. M., Duda, M. G., et al. (2008). A description of the Advanced Research WRF version 3, *NCAR Tech. Note NCAR/TN-475+STR* (p 113). https://doi.org/10.5065/D68S4MVH

Sun, Y., Chen, C., Beardsley, R. C., Xu, Q., Qi, J., & Lin, H. (2013). Impact of current-wave interaction on storm surge simulation: A case study for Hurricane Bob. *Journal of Geophysical Research: Oceans*, *118*, 2685–2701. https://doi.org/10.1002/jgrc.20207

Tiedtke, M. (1989). A comprehensive mass flux scheme for cumulus parameterization in large-scale models. *Monthly Weather Review*, *117*(8), 1779–1800. https://doi.org/10.1175/1520-0493(1989)117<1779:ACMFSF>2.0.CO;2

Wang, Z.-Q., & Duan, A.-M. (2012). A new ocean mixed-layer model coupled into WRF. *Atmospheric and Oceanic Science Letters*, *5*(3), 170–175. https://doi.org/10.1080/16742834.2012.11446988

Warner, J. C., Armstrong, B., He, R., & Zambon, J. B. (2010). Development of a Coupled Ocean-Atmosphere-Wave-Sediment Transport (COAWST) modeling system. *Ocean Modelling*, *35*(3), 230–244. https://doi.org/10.1016/j.ocemod.2010.07.010

Warner, T. T. (2011). Quality assurance in atmospheric modeling. *Bulletin of the American Meteorological Society*, *92*(12), 1601–1610. https://doi.org/10.1175/BAMS-D-11-00054.1

Wu, C.-C., Lee, C.-Y., & Lin, I.-I. (2007). The effect of the ocean eddy on tropical cyclone intensity. *Journal of the Atmospheric Sciences*, *64*(10), 3562–3578. https://doi.org/10.1175/JAS4051.1

Wu, C.-C., Tu, W.-T., Pun, I.-F., Lin, I.-I., & Peng, M. S. (2016). Tropical cyclone-ocean interaction in Typhoon Megi (2010)—A synergy study based on ITOP observations and atmosphere-ocean coupled model simulations. *Journal of Geophysical Research: Atmospheres*, *121*, 153–167. https://doi.org/10.1002/2015JD024198

Zambon, J. B., He, R., & Warner, J. C. (2014). Tropical to extratropical: Marine environmental changes associated with Superstorm Sandy prior to its landfall. *Geophysical Research Letters*, *41*, 8935–8943. https://doi.org/10.1002/2014GL061357

Zeng, X., & Beljaars, A. (2005). A prognostic scheme of sea surface skin temperature for modeling and data assimilation. *Geophysical Research Letters*, *32*, L14605. https://doi.org/10.1029/2005GL023030

Zhang, F., & Li, M. (2019). Impacts of ocean warming, sea level rise, and coastline management on storm surge in a semienclosed bay. *Journal of Geophysical Research: Oceans*, *124*, 6498–6514. https://doi.org/10.1029/2019JC015445

Zhang, Y., Chen, C., Beardsley, R. C., Gao, G., Lai, Z., Curry, B., et al. (2016). Studies of the Canadian Arctic Archipelago water transport and its relationship to basin-local forcings: Results from AO-FVCOM. *Journal of Geophysical Research: Oceans*, *121*, 4392–4415. https://doi.org/10.1002/2016JC011634

Zhang, Y., Chen, C., Beardsley, R. C., Gao, G., Qi, J., & Lin, H. (2016). Seasonal and interannual variability of the Arctic sea ice: A comparison between AO-FVCOM and observations. *Journal of Geophysical Research: Oceans*, *121*, 8320–8350. https://doi.org/10.1002/2016JC011841

Zou, X., & Xiao, Q. (2000). Studies on the initialization and simulation of a mature hurricane using a variational bogus data assimilation scheme. *Journal of the Atmospheric Sciences*, *57*(6), 836–860. https://doi.org/10.1175/1520-0469(2000)057<0836:SOTIAS>2.0.CO;2